Vertical Plasmonic Mach-Zehnder interferometer for sensitive optical sensing

Qiaoqiang Gan[1], Yongkang Gao, Filbert J. Bartoli[*]

Center for Optical Technologies, Electrical and Computer Engineering Department *Lehigh University, Bethlehem, PA 18015, USA*

[1]qig206@lehigh.edu

**fjb205@lehigh.edu*

Abstract: Vertical plasmonic Mach-Zehnder Interferometers are investigated theoretically and experimentally, and their potential for ultra-sensitive optical sensing is discussed. Plasmonic interferences arise from coherently coupled pairs of subwavelength slits, illuminated by a broadband optical source, and this interference modulates the intensity of the far-field scattering spectrum. Experimental results, obtained using a simple experimental setup, are presented to validate theoretically predicted interferences introduced by the surface plasmon modes on top and bottom surfaces of a metal film. By observing the wavelength shift of the peaks or valleys of the interference pattern, this highly compact device has the potential to achieve a very high sensitivity relative to other nanoplasmonic architectures reported.

OCIS codes: (240.6680) Surface plasmons; (260.3910) Metals, optics of; (130.6010) Sensors; (310.2790) Guided waves.

References and links

1. J. Homola, "Surface plasmon resonance sensors for detection of chemical and biological species," Chem. Rev. **108**(2), 462–493 (2008).
2. M. E. Stewart, C. R. Anderton, L. B. Thompson, J. Maria, S. K. Gray, J. A. Rogers, and R. G. Nuzzo, "Nanostructured plasmonic sensors," Chem. Rev. **108**(2), 494–521 (2008).
3. J. N. Anker, W. P. Hall, O. Lyandres, N. C. Shah, J. Zhao, and R. P. Van Duyne, "Biosensing with plasmonic nanosensors," Nat. Mater. **7**(6), 442–453 (2008).
4. M. E. Stewart, N. H. Mack, V. Malyarchuk, J. A. N. Soares, T. W. Lee, S. K. Gray, R. G. Nuzzo, and J. A. Rogers, "Quantitative multispectral biosensing and 1D imaging using quasi-3D plasmonic crystals," Proc. Natl. Acad. Sci. U.S.A. **103**(46), 17143–17148 (2006).
5. J. C. Yang, J. Ji, J. M. Hogle, and D. N. Larson, "Metallic nanohole arrays on fluoropolymer substrates as small label-free real-time bioprobes," Nano Lett. **8**(9), 2718–2724 (2008).
6. K. A. Tetz, L. Pang, and Y. Fainman, "High-resolution surface Plasmon resonance sensor based on linewidth-optimized nanohole array transmittance," Optim. Lett. **31**(10), 1528 (2006).
7. A. Lesuffleur, H. Im, N. C. Lindquist, and S. H. Oh, "Periodic nanohole arrays with shape-enhanced Plasmon resonance as real-time biosensors," Appl. Phys. Lett. **90**(24), 243110 (2007).
8. A. G. Brolo, R. Gordon, B. Leathem, and K. L. Kavanagh, "Surface plasmon sensor based on the enhanced light transmission through arrays of nanoholes in gold films," Langmuir **20**(12), 4813–4815 (2004).
9. A. De Leebeeck, L. K. Kumar, V. de Lange, D. Sinton, R. Gordon, and A. G. Brolo, "On-chip surface-based detection with nanohole arrays," Anal. Chem. **79**(11), 4094–4100 (2007).
10. J. C. Sharpe, J. S. Mitchell, L. Lin, N. Sedoglavich, and R. J. Blaikie, "Gold nanohole array substrates as immunobiosensors," Anal. Chem. **80**(6), 2244–2249 (2008).
11. G. M. Hwang, L. Pang, E. H. Mullen, and Y. Fainman, "Plasmonic sensing of biological analytes through nanoholes," IEEE Sens. J. **8**(12), 2074–2079 (2008).
12. J. Henzie, M. H. Lee, and T. W. Odom, "Multiscale patterning of plasmonic metamaterials," Nat. Nanotechnol. **2**(9), 549–554 (2007).
13. J. Ji, J. G. O'Connell, D. J. Carter, and D. N. Larson, "High-throughput nanohole array based system to monitor multiple binding events in real time," Anal. Chem. **80**(7), 2491–2498 (2008).
14. H. Im, A. Lesuffleur, N. C. Lindquist, and S. H. Oh, "Plasmonic nanoholes in a multichannel microarray format for parallel kinetic assays and differential sensing," Anal. Chem. **81**(8), 2854–2859 (2009).
15. J. Ji, J. C. Yang, and D. N. Larson, "Nanohole arrays of mixed designs and microwriting for simultaneous and multiple protein binding studies," Biosens. Bioelectron. **24**(9), 2847–2852 (2009).
16. D. Braun, and P. Fromherz, "Fluorescence interferometry of neuronal cell adhesion on microstructured silicon," Phys. Rev. Lett. **81**(23), 5241–5244 (1998).

#117905 - $15.00 USD Received 29 Sep 2009; revised 12 Oct 2009; accepted 12 Oct 2009; published 28 Oct 2009

17. L. Moiseev, M. S. Unlü, A. K. Swan, B. B. Goldberg, and C. R. Cantor, "DNA conformation on surfaces measured by fluorescence self-interference," Proc. Natl. Acad. Sci. U.S.A. **103**(8), 2623–2628 (2006).
18. A. Bilenca, J. Cao, M. Colice, A. Ozcan, B. Bouma, L. Raftery, and G. Tearney, "Fluorescence interferometry: principles and applications in biology," Ann. N. Y. Acad. Sci. **1130**(1), 68–77 (2008).
19. M. Dogan, A. Yalcin, S. Jain, M. B. Goldberg, A. K. Swan, M. S. Unlu, and B. B. Goldberg, "Spectral Self-Interference Fluorescence Microscopy for Subcellular Imaging," IEEE J. Sel. Top. Quantum Electron. **14**(1), 217–225 (2008).
20. G. Shtengel, J. A. Galbraith, C. G. Galbraith, J. Lippincott-Schwartz, J. M. Gillette, S. Manley, R. Sougrat, C. M. Waterman, P. Kanchanawong, M. W. Davidson, R. D. Fetter, and H. F. Hess, "Interferometric fluorescent super-resolution microscopy resolves 3D cellular ultrastructure," Proc. Natl. Acad. Sci. U.S.A. **106**(9), 3125–3130 (2009).
21. F. Brosinger, H. Freimuth, M. Lacher, W. Ehrfeld, E. Gedig, A. Katerkamp, F. Spener, and K. Cammann, "A label-free affinity sensor with compensation of unspecific protein interaction by a highly sensitive integrated optical Mach–Zehnder interferometer on silicon," Sens. Actuators B Chem. **44**(1-3), 350–355 (1997).
22. F. Prieto, B. Sepulveda, and A. Calle, A. Llobera, C. Dominguez, A. Abad, A. Montoya and L. M. Lechuga, "An integrated optical interferometric nanodevice based on silicon technology for biosensor applications," Nanotechnology **14**(8), 907–912 (2003).
23. F. Prieto, B. Sepulveda, A. Calle, A. Llobera, C. Dommguez, and L. M. Lechuga, "Integrated Mach–Zehnder interferometer based on ARROW structures for biosensor applications," Sens. Actuators B Chem. **92**(1-2), 151–158 (2003).
24. E. F. Schipper, A. M. Brugman, L. M. Lechuga, R. P. H. Kooyman, J. Greve, and C. Dominguez, "The realization of an integrated Mach-Zehnder waveguide immunosensor in silicon technology," Sens. Actuators B Chem. **40**(2-3), 147–153 (1997).
25. A. Ymeti, J. S. Kanger, J. Greve, P. V. Lambeck, R. Wijn, and R. G. Heideman, "Realization of a multichannel integrated Young interferometer chemical sensor," Appl. Opt. **42**(28), 5649–5660 (2003).
26. M. J. Swann, L. L. Peel, S. Carrington, and N. J. Freeman, "Dual-polarization interferometry: an analytical technique to measure changes in protein structure in real time, to determine the stoichiometry of binding events, and to differentiate between specific and nonspecific interactions," Anal. Biochem. **329**(2), 190–198 (2004).
27. D. J. Bornhop, J. C. Latham, A. Kussrow, D. A. Markov, R. D. Jones, and H. S. Sørensen, "Free-solution, label-free molecular interactions studied by back-scattering interferometry," Science **317**(5845), 1732–1736 (2007).
28. E. Ozkumur, J. W. Needham, D. A. Bergstein, R. Gonzalez, M. Cabodi, J. M. Gershoni, B. B. Goldberg, and M. S. Unlü, "Label-free and dynamic detection of biomolecular interactions for high-throughput microarray applications," Proc. Natl. Acad. Sci. U.S.A. **105**(23), 7988–7992 (2008).
29. H. F. Schouten, N. Kuzmin, G. Dubois, T. D. Visser, G. Gbur, P. F. Alkemade, H. Blok, G. W. Hooft, D. Lenstra, and E. R. Eliel, "Plasmon-assisted two-slit transmission: Young's experiment revisited," Phys. Rev. Lett. **94**(5), 053901 (2005).
30. V. V. Temnov, U. Woggon, J. Dintinger, E. Devaux, and T. W. Ebbesen, "Surface Plasmon interferometry: measuring group velocity of surface plasmons," Optim. Lett. **32**(10), 1235 (2007).
31. X. Wu, J. Zhang, J. Chen, C. Zhao, and Q. Gong, "Refractive index sensor based on surface-plasmon interference," Optim. Lett. **34**(3), 392 (2009).
32. M. H. Lee, H. Gao, and T. W. Odom, "Refractive index sensing using quasi one-dimensional nanoslit arrays," Nano Lett. **9**(7), 2584–2588 (2009).
33. E. D. Palik, Handbook of Optical Constants of Solids (Aacademic, Orlando, LF, 1985), **Vol. 1**.
34. Z. Fu, and Q. Gan, K. Gao, G. Wang, Z. Pan, F. Bartoli,. "Numerical Investigation of a Bidirectional Wave Coupler Based on Surface Plasmonic Polarition Bragg Gratings in Near Infrared Spectrum," J. Lightwave Technol. **26**, 3699 (2008).
35. Q. Gan, Z. Fu, Y. J. Ding, and F. J. Bartoli, "Ultrawide-bandwidth slow-light system based on THz plasmonic graded metal grating structures," Phys. Rev. Lett. **100**(25), 256803 (2008).
36. Q. Gan, Y. J. Ding, and F. J. Bartoli, "Rainbow" trapping and releasing at telecommunication wavelengths," Phys. Rev. Lett. **102**(5), 056801 (2009).
37. P. Lalanne, J. P. Hugonin, and J. C. Rodier, "Approximate model for surface-plasmon generation at slit apertures," J. Opt. Soc. Am. B **23**(7), 1608 (2006).
38. H. W. Kihm, G. K. Lee, D. S. Kim, J. H. Kang, and P. Q. Han, "Control of surface Plasmon generation efficiency by silt-width tuning," Appl. Phys. Lett. **92**(5), 051115 (2008).
39. A. Drezet, A. Hohenau, A. L. Stepanov, H. Ditlbacher, B. Steinberger, N. Galler, F. R. Aussenegg, A. Leitner, and J. R. Krenn, "How to erase surface plasmon fringes," Appl. Phys. Lett. **89**(9), 091117 (2006).
40. P. Lalanne, and J. P. Hugonin, "Interaction between optical nano-objects at metallo-dielectric interfaces," Nat. Phys. **2**(8), 551–556 (2006).
41. F. J. García de Abajo; F. J Garcia de Abajo, "Light scattering by particle and hole arrays," Rev. Mod. Phys. **79**(4), 1267–1290 (2007).
42. J. Weiner, "The physics of light transmission through subwavelength apertures and aperture arrays," Rep. Prog. Phys. **72**(6), 064401 (2009).
43. P. Lalanne, J. P. Hugonin, H. T. Liu, and B. Wang, A microscopic view of the electromagnetic properties of sub-λ metallic surfaces, Surf. Sci. Rep. (2009).

#117905 - $15.00 USD Received 29 Sep 2009; revised 12 Oct 2009; accepted 12 Oct 2009; published 28 Oct 2009

1. Introduction

Surface Plasmons (SPs) are coherent oscillations of conduction electrons on a metal surface excited by electromagnetic radiation at the metal-dielectric interface. The sensitivity of the Surface Plasmon Resonance (SPR) to the refractive index change at a flat metal interface has led to the development of SPR sensing systems, which typically use prisms to couple light into a single surface-plasmon mode on a flat, continuous metal film (typically gold) [1]. However the intrinsic size of these experimental systems is a disadvantage for applications requiring integrated, low-cost, compact, image-based devices for portable, rapid bioanalytical measurements. Nanoplasmonic biosensors, employing nanoscale metal particles and nanostructured hole arrays, slits or gratings, and other novel topographies, could be an attractive miniaturized platform for sensitive, label-free monitoring of cellular processes [1–3]. When receptor molecules are immobilized on the nanostructured metal surface, the binding of target biomolecules changes the local refractive index, affecting the optical properties of the SP modes and permitting optical detection [4,5]. Recent advances in nanofabrication, nanomaterial synthesis, and nanocharacterization permit significant advances over conventional SPR evanescent wave-based biosensors, whose large size limits their effectiveness for probing nanovolumes and single cells, and for integration into microfluidic platforms. In recent years, periodic nanoplasmonic structures have been successfully employed in biosensing applications [4–15]. However, the sensitivities for these nanoplasmonic structures reported to date are much lower (two to three orders of magnitude) than other sensitive optical sensing technologies [1,4–15]. Consequently, increasing the sensitivity of nanoplasmonic biosensors is essential to their integration into practical devices and achieving significant impact on the future markets.

Interferometry is one of the most sensitive optical interrogation methods and has been used to screen molecular interactions in surface binding modes. Examples include fluorescence interferometry for high resolution microscopy or nanoscopy [16–20], label-free sensing based on the Mach-Zehnder Interferometer (MZI) [21–24], Young Interferometer [25], dual polarization interferometer [26], back-scattering interferometry [27], and spectral reflectance interferometry [28], etc. Recently, surface plasmon interferometry was also proposed [29,30], and is believed to be promising for sensitive lable-free sensing applications [31].

In this article, we propose a vertical plasmonic Mach-Zehnder interferometer (VPMZI) for sensitive optical sensing. The paper is organized as follows. We first investigate the principle of operation for the VPMZI in section 2. Section 3 presents analytical calculations and numerical simulations, and discusses how high sensitivity may be achieved by combining SP modes with the MZI concept. We show that the sensitivity of compact biosensing devices could be enhanced significantly relative to other nanoplasmonic architectures reported [4–15] when the refractive indices at the top and bottom surfaces of the metal film are closely matched. To complement the theoretical investigations, we present in section 4 experimental observation of the spectral interference introduced by the VPMZI. The experimental apparatus is relatively simple, and the measured results indicate that SPP modes at the top and bottom surfaces do interfere with each other and have the potential to achieve high sensitivity to the surface refractive index change. Finally, conclusions and potential applications of the VPMZI are presented in Section 5.

2. VPMZI Constructed by double slits on a metal film

We consider the structure illustrated in the upper inset in Fig. 1, which contains two nanoslits in a metal film deposited on a glass substrate. In principle, both the top surface (1: liquid/metal interface) and bottom surface (2: metal/glass interface) can support SPP modes. When SPP modes excited by the slit at the right propagate to the left slit, the SPP signals from the two optical branches (the top and bottom interfaces) interfere with each other and modulate the far-field scattering, essentially comprising a plasmonic MZI. The sensing arm of this plasmonic MZI is on the top surface of the metal film, and the reference arm is at the

#117905 - $15.00 USD Received 29 Sep 2009; revised 12 Oct 2009; accepted 12 Oct 2009; published 28 Oct 2009

bottom surface. Because of the relative position of these two arms, which is vertical to the metal surface, we call it a vertical plasmonic MZI. The expression for the far-field interference pattern contains the term $\cos\left[\frac{2\pi L}{\lambda}\left(\sqrt{\frac{\varepsilon_m'(\lambda)n_1^2}{\varepsilon_m'(\lambda)+n_1^2}}-\sqrt{\frac{\varepsilon_m'(\lambda)n_2^2}{\varepsilon_m'(\lambda)+n_2^2}}\right)\right]$. [31]. Here, ε'_m is the real part of the metal permittivity, n_1 is the refractive index of the dielectric material on top of the metal surface, n_2 is the refractive index of the substrate, and L is the slit separation distance. The term $\sqrt{\frac{\varepsilon_m'(\lambda)n^2}{\varepsilon_m'(\lambda)+n^2}}$ is the effective refractive index (ERI) of the metal/dielectric interface. Notably, the two branches of this plasmonic MZI structure comprise a vertical structure, which differs from conventional planar MZI devices [21–24]. An advantage of this VPMZI is that this vertical integration permits denser array packing. The gap between the sensing and reference arms is only several hundred nanometers, which is appreciably smaller than for silicon-based planar MZIs. In addition, this structure, which consists of double slits in a metal film, should be quite simple to fabricate in large-area arrays [32].

The phase modulation properties of this novel VPMZI are sensitive to changes in the refractive index in the sensing arm (top surface) relative to that in the reference arm (bottom surface). When the refractive index of the sensing arm, n_1, is changed to $n_1 + \Delta n_1$, the phase change is given by the expression

$$\Delta\phi = \frac{2\pi L}{\lambda}\left(\sqrt{\frac{\varepsilon_m'(\lambda)n_1^2}{\varepsilon_m'(\lambda)+n_1^2}}-\sqrt{\frac{\varepsilon_m'(\lambda)(n_1+\Delta n_1)^2}{\varepsilon_m'(\lambda)+(n_1+\Delta n_1)^2}}\right) \quad (1)$$

which relates the phase change to the change in refractive index. In our calculations, an incident wavelength of 1033nm is employed, for which the permittivity of silver is $-48.81 + i3.16$ [33]. We assume that the dielectric material on the sensing surface is water ($n_1 = 1.33$) and the slit separation distance, L, is 70μm. As shown in Fig. 1, a refractive index change of 0.1 may introduce a phase change of about $7.2(2\pi)$, which is in a good agreement with the two-dimensional (2D) finite-difference-time-domain (FDTD) modeling result shown in the lower inset of Fig. 1. Based on the FDTD modeling result, more than 7 periods of the interference pattern can be observed in the far-field scattering signal, which can be utilized in optical sensing applications. However, the length of the sensing arm for this metal structure must be kept short due to the intrinsic loss of metals. Consequently, the phase-change sensitivity of this metallic MZI [~$72(2\pi)$/RIU] is much lower than Si-based MZI devices with very long sensing arms [21–24]. For example, the phase-change sensitivity of a Si-based MZI with a 5mm sensing arm was reported to be about $1400(2\pi)$/RIU [24].

#117905 - $15.00 USD Received 29 Sep 2009; revised 12 Oct 2009; accepted 12 Oct 2009; published 28 Oct 2009

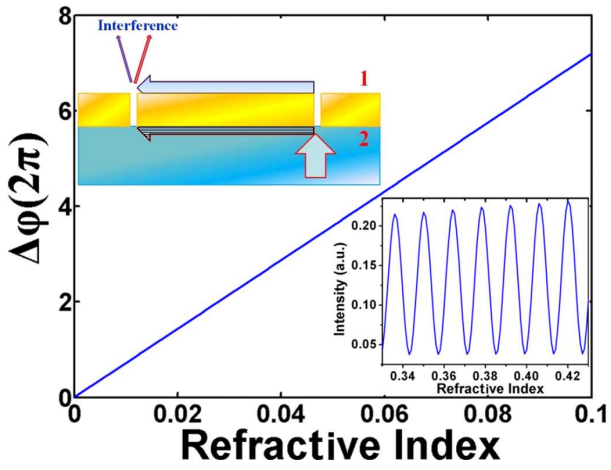

Fig. 1. The phase modulation properties of VPMZI. The upper inset: The interference path related to the SPP modes on the top and bottom interfaces. The lower inset: Intensity modulation output signal from the VPMZI modeled by FDTD simulations.

3. Achieving high sensitivity by matching the refractive indices at the two surfaces

Besides the phase modulation at a single wavelength, such double-slit or slit-groove metal structures have also been reported to exhibit spectral interference when the input is a broad band light source [29–31]. In this section, we discuss how that the spectral interference supported by this proposed VPMZI can lead to an high sensitivity, significantly better than that reported for other nanoplasmonic architectures [4–15,32].

When the refractive index of the dielectric top layer is changed, the peaks and valleys in the interference pattern will shift accordingly. The sensitivity could be approximately derived by setting the term. $\frac{2\pi L}{\lambda}\left(\sqrt{\frac{\varepsilon_m'(\lambda)n_1^2}{\varepsilon_m'(\lambda)+n_1^2}}-\sqrt{\frac{\varepsilon_m'(\lambda)n_2^2}{\varepsilon_m'(\lambda)+n_2^2}}\right)$.to be constant, yielding [31]:

$$S=\frac{\Delta\lambda}{\Delta n}=\frac{\lambda}{n_1^3}\left(\frac{\varepsilon_m'(\lambda)n_1^2}{\varepsilon_m'(\lambda)+n_1^2}\right)^{3/2}\Bigg/\left(\sqrt{\frac{\varepsilon_m'(\lambda)n_1^2}{\varepsilon_m'(\lambda)+n_1^2}}-\sqrt{\frac{\varepsilon_m'(\lambda)n_2^2}{\varepsilon_m'(\lambda)+n_2^2}}\right) \qquad (2)$$

From Eq. (2), it is seen that when the $n_1 < n_2$, the sensitivity parameter is negative, indicating that the interference pattern will shift to shorter wavelengths, whereas if $n_1 > n_2$, the sensitivity value is positive, indicating that the interference pattern will shift to longer wavelengths. More importantly, this equation indicates that the sensitivity increases greatly if the two terms in the denominator are close in value. Figure 2 illustrates the sensitivities that could potentially be achieved by varying the refractive index of the substrate material below the metal surface. In this calculation, we assume the metal film is gold and the top dielectric layer is water (n_1 = 1.33). As an example, when n_2 = 1.51, the relation between the sensitivity and the operating wavelength is shown by the lowest curve in Fig. 2. These simulation parameters, which are similar to the measurement conditions employed in ref [31], yielded a sensitivity of approximately 4718nm/RIU at approximately 860nm. This value is in close agreement with experimental value of 4547nm/RIU reported in ref [31]. Based on Eq. (2), Wu *et. al.* noted that higher sensitivities can be achieved at longer wavelengths [31]. However, this approach to improving performance is limited by strong water absorption in the near-infrared spectral region. Another obvious approach to enhance the sensitivity, not emphasized in ref [31], can be realized when the refractive index of the substrate, n_2, is decreased, approaching that of the top layer, n_1, as illustrated by the series of curves in Fig. 2.

#117905 - $15.00 USD Received 29 Sep 2009; revised 12 Oct 2009; accepted 12 Oct 2009; published 28 Oct 2009

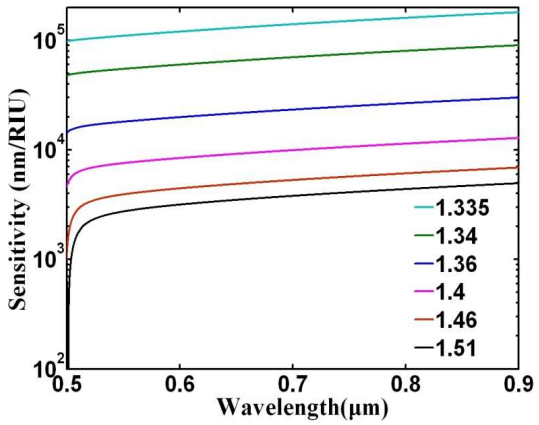

Fig. 2. Theoretical sensitivity (absolute value) of the VPMZI obtained by Eq. (1). The thickness of the Au film is 200nm. The gap between the two slits is 70μm, and the width of each slit is 400nm. In this calculation, the refractive index for the top layer is 1.33.

The most important design requirement for a sensitive VPMZI is to match the ERI at the top and bottom interfaces. The ideal structure to meet the ERI matching condition is the one where the dispersion curve at the top surface is very close to that at the bottom interface, indicating that the ERI match condition could be met over a broad range of wavelengths. This can in principle be accomplished by finding a substrate whose refractive index is close to the liquid on the top. For example, the authors in ref [5] employed the fluorinated ethylene propylene copolymer (FEP) as a replica substrate because it is chemically inert, thermoplastic, transparent in the visible region, and has a refractive index of 1.341 at the λ of 590 nm. Here we employ the 2D FDTD method to simulate the sensitivity for a Au structure on substrates with various values of refractive index. The computational setup is shown in the upper inset in Fig. 1, the separation between the two slits is 70μm. Only one slit is illuminated by the incident light. The scattered light from the other slit is monitored. One can calculate the sensitivity from the shift in the peak or valley wavelength. For example, consider n_2 = 1.46. When n_1 changes from 1.33 to 1.331, the peak of the interference pattern at 970nm will shift to 964nm, indicating that the sensitivity is $-0.6\text{X}10^4$ nm/RIU [see the upper panel in Fig. 3(a)]. If n_2 is instead set to 1.36, the valley of the interference pattern at 940nm will shift to 908nm, indicating a sensitivity of about $-3.2\text{X}10^4$nm/RIU. Similarly, the peak at 1168nm will shift to 1132nm, indicating a sensitivity of about $-3.6\text{X}10^4$nm/RIU [see the upper panel in Fig. 3(b)]. When n_2 is further decreased to 1.35, the valley position at 1076nm will shift to 1034nm, indicating a sensitivity of $-4.2\text{X}10^4$nm/RIU. At the same time, the peak at 1582nm will shift to 1486nm, indicating a sensitivity of about $-9.2\text{X}10^4$nm/RIU [see the upper panel in Fig. 3(c)]. Using the interference expression, $\frac{2\pi L}{\lambda}\left(\sqrt{\frac{\varepsilon_m'(\lambda)n_1^2}{\varepsilon_m'(\lambda)+n_1^2}}-\sqrt{\frac{\varepsilon_m'(\lambda)n_2^2}{\varepsilon_m'(\lambda)+n_2^2}}\right)$, the theoretical spectral interference pattern of this structure was calculated and plotted in the lower panels in Fig. 3, which is in reasonably good agreement with the FDTD modeling result. Remarkably, the sensitivities shown in Fig. 3 (b) and (c) are between one and two orders of magnitude larger than the best sensitivity reported for nanohole arrays in ref [11] (about 1500nm/RIU).

#117905 - $15.00 USD Received 29 Sep 2009; revised 12 Oct 2009; accepted 12 Oct 2009; published 28 Oct 2009

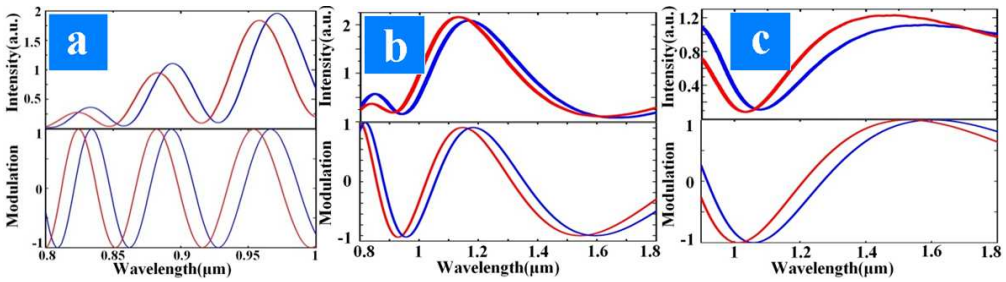

Fig. 3. Numerical modeling for the interference signal of the scattered light from the slit on the Au film shown in Fig. 1 (a). The refractive indices of the substrates are 1.46 (a), 1.36 (b) and 1.35 (c), respectively. The gap between the two slits is fixed to be 70μm. The upper panels are FDTD modeling results, and the lower panels are results obtained using the term $\cos\left[\frac{2\pi L}{\lambda}\left(\sqrt{\frac{\varepsilon_m'(\lambda)n_1^2}{\varepsilon_m'(\lambda)+n_1^2}}-\sqrt{\frac{\varepsilon_m'(\lambda)n_2^2}{\varepsilon_m'(\lambda)+n_2^2}}\right)\right]$.

If a low refractive index substrate is unavailable, the ERI matching condition can also be met by various surface dispersion engineering approaches. For example, one can introduce a thin film of dielectric material with a higher refractive index on top of the metal surface to tune the ERI of this interface. Various nanopatterned structures, such as periodic metal-dielectric-air grooves [34] and surface grating structures [35,36], could also be employed to finely tune the shape of the dispersion curve and approach to the ERI match condition. In addition to optimizing the sensitivity, other important factors should be considered, such as fluctuations in the refractive index induced by changes in temperature, which were not considered in this theoretical study. Considering that the temperature induced refractive index changes for SiO_2 substrates and metals are smaller than that for Si-based waveguides, the temperature performance of this plasmonic MZI is expected to be better than Si-based MZI devices. This will be studied further in future investigations.

4. Experimental validation of the spectral interference in the VPMZI

In the previous sections, we discussed predictions that measurement of the spectral interference in a VPMZI can lead to very high sensitivity. We now discuss the important question of how straightforward it may be to observe the SPP-mediated spectral interference experimentally. In a previous report, Wu *et. al.* employed a prism based SPR apparatus using a tunable Ti-Sapphire laser [31] to observe spectral interference patterns. Here we present a simpler experimental approach to measure spectral interferences and to validate theoretical predictions for the VPMZI.

#117905 - $15.00 USD Received 29 Sep 2009; revised 12 Oct 2009; accepted 12 Oct 2009; published 28 Oct 2009

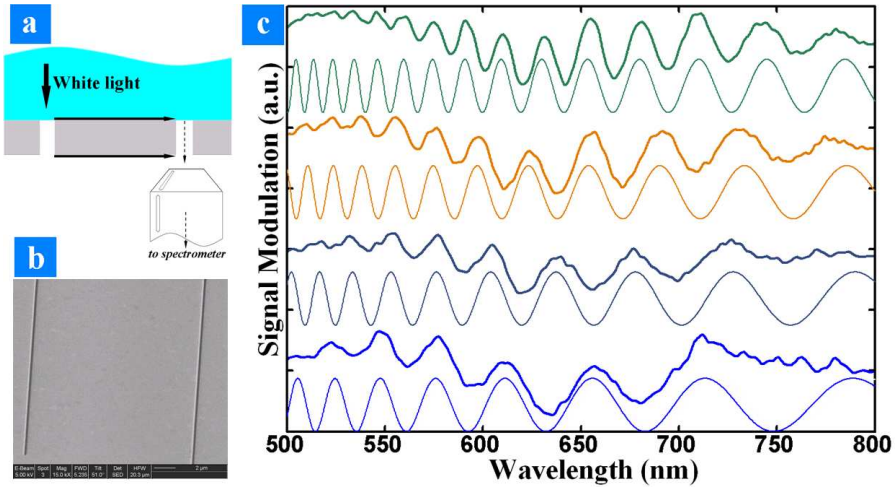

Fig. 4. (a) Sketch of the doublet geometry. (b) A scanning electron microscope image of a doublet structure with a slit–slit separation distance of 15.73μm. (c) SPP-mediated spectral interference introduced by the SPP modes from the top and bottom surfaces: Here we study 4 doublet samples on a Ag film with slit–slit separation distances of 10.50μm (bottom), 13.12μm (lower center), 15.73μm (upper center) and 20.98μm (top). Bold solid lines are measurement results and the thin solid lines are theoretical predictions.

The optical transmission measurements were performed using an Olympus X81 inverted microscope. A white light beam from a 100W Halogen lamp was focused at normal incidence onto the sample surface (glass substrate side) through the microscope condenser with a linear polarizer. The polarization of the incident light is either parallel (TE) or perpendicular (TM) to the long axis of the slit. The transmission light was collected by a X40 microscope objective with a numerical aperture of 0.6. The collected light was coupled into a multimode fiber bundle interfaced to a fiber-based compact spectrometer (Ocean Optics USB 4000). A CCD camera was employed to align the position of the double slits, ensuring nearly identical collection conditions for all samples studied. An illustration of the doublet geometry is shown in Fig. 4 (a). The white light beam is focused at one of the slits. A diaphragm in the condenser was employed to control the intensity of the light beam illuminating the other slit. A series of surface-wave interferometers, consisting of double slits with varying slit–slit separation distances, were fabricated by FIB milling (FEI Dual-Beam system 235) on 300nm-thick layers of Ag (or Au) evaporated onto flat fused silica microscope slides (Fisherbrand). Here we examine 4 doublet samples on a Ag film with slit–slit separation distances of 10.50, 13.12, 15.73 and 20.98μm. A scanning electron microscope image of a doublet structure with a slit–slit separation distance of 15.73μm is shown in Fig. 4 (b). The width of the slit is about 220nm. The measurement results are shown by bold solid lines in Fig. 4 (c). Obvious spectral interference patterns are observed under the TM illumination. In this plot, the low frequency background and high frequency noise have been numerically filtered using a Fast Fourier Transform technique (here we set the low frequency cutoff at ~2.896μm^{-1} and the high frequency cutoff at ~217.196μm^{-1}). To interpret these measurements, theoretical interference patterns are calculated using the term $\cos\left[\frac{2\pi L}{\lambda}\left(\sqrt{\frac{\varepsilon_m'(\lambda)n_1^2}{\varepsilon_m'(\lambda)+n_1^2}}-\sqrt{\frac{\varepsilon_m'(\lambda)n_2^2}{\varepsilon_m'(\lambda)+n_2^2}}\right)\right]$ [see the thin solid lines in Fig. 4 (c)]. One can see the theoretical predictions agree very well with the measured data, indicating that the SPP-mediated spectral interference from the top and bottom surfaces is clearly observed in this simple experiment. It should be noted that such an air/Ag/glass interface is capable of supporting several different interference patterns: the SPP modes on interface 1 or interface 2 [see the inset in Fig. (1)] can both interfere with the free space light and introduce interference patterns with higher modulation frequencies [29,30]. In our measurements, these higher frequency modulation signals were also observed, for example, in

#117905 - $15.00 USD Received 29 Sep 2009; revised 12 Oct 2009; accepted 12 Oct 2009; published 28 Oct 2009

the wavelength region from 700nm to 800nm. To optimize the amplitude of the interference signal, the intensity of the two SPP modes should be carefully balanced. This involves the coupling efficiencies for the two SPP modes at the top and bottom surfaces in a single sample. It was proposed that the SPP coupling efficiency can be tuned by varying the slit width [37]. The performance of the VPMZI could be optimized further by varying the widths of the slits, the separation distance between the slits, and the refractive indices of the materials on top and bottom of the metal film. A more detailed experimental analysis of these issues is still under investigation and will be discussed elsewhere. Compared with previous reports that employ more complex instrumentation (such as near-field scanning microscope [38], leakage radiation microscope [39], and a prism-based SPR setup [31], etc.), our measurement apparatus is relatively simple and the measurements are easy to repeat. Such measurements are also very useful for gaining deeper insight into the SPP-mediated interaction between optical nano-objects at metallo-dielectric interfaces [40–43].

5. Conclusion

In conclusion, this work demonstrates the feasibility of the VPMZI with very high sensitivity for optical sensing, and a potential one-to-two orders-of-magnitude improvement over previously reported nanoaperture arrays. Plasmonic interferences arise from coherently coupled pairs of subwavelength slits, illuminated from below by an optical beam, and this interference modulates the intensity of the far-field scattering. A simple experiment setup is also presented to observe the spectral interference introduced by the SPP modes from the two surfaces. Important advantages of this design were discussed, including the vertical MZI structure, in which the sensing branch is on top of the metal-liquid interface, and the reference branch is on the bottom interface. The gap between these two branches is only tens or hundreds of nanometers, which is promising for novel integrated sensitive biosensing platforms and subwavelength optics on-a-chip.

Acknowledgment

The authors would like to acknowledge the support of this research by NSF (Award # 0901324).

#117905 - $15.00 USD Received 29 Sep 2009; revised 12 Oct 2009; accepted 12 Oct 2009; published 28 Oct 2009